Research Article

Amon Kimeli*, Oliver Ocholla, Judith Okello, Nico Koedam, Hildegard Westphal, and
James Kairo

# Geochemical and petrographic characteristics of sediments along the transboundary (Kenya–Tanzania) Umba River as indicators of provenance and weathering

**Abstract:** The Umba River basin is one of the smaller-scale hydrological basins in the East African region. It traverses two countries, with its catchment in the Usambara mountains in Tanzania, while it drains its waters to the Indian Ocean in Vanga, Kenya. The chemical and mineralogical compositions of the riverbank and bottom sediments of the Umba River were analyzed and evaluated to describe their source characteristics and provenance. The dominant minerals include quartz, K-feldspars, plagioclase, hornblende, pyroxenes, muscovite, biotite, and likely presence of clays such as kaolinite. The chemical index of alteration of the sediments indicate a moderate to high degree of alteration. They reflect a dominant mafic to intermediate igneous provenance consistent with the geology of the Umba River catchment that is characterized by the outcrops of the granitic Precambrian basement and the quartz-dominated Paleozoic Karoo Supergroup, overlain by Mesozoic and Cenozoic sediments dominated by both mafic and felsic minerals. The similarity of the chemical and mineralogical compositions of the Umba River sediments from source to mouth further indicates a uniform source in the upper course of the river and only subordinate contributions from the lower course where it passes the Karoo and the younger sediments.

## 1 Introduction

Rivers deliver large amounts of terrigenous sediments into the global oceans [1]. These sediments play a vital role in both the earth surface processes and the biogeochemical cycle. Fluvial sediments are typically heterogeneous being composed of weathered and eroded rocks along the river's course and are subsequently altered during downstream transportation. These alteration processes are generally characterized as either physical (e.g., fragmentation, abrasion, and attrition) or chemical (e.g., dissolution, decay, and adsorption) [2,3]. The final chemical sediment composition can be different from the source material because of secondary processes during fluvial transport, deposition, and post-depositional early diagenesis [4,5]. The rate of alteration of fluvial sediments is influenced by several factors including the primary composition determined by the source geology, climatic conditions, topography and thus water energy, vegetation, transported distance, and human activities (e.g., land use and construction) [6]. The mineralogical and chemical resemblance to the source rock is higher in sediments transported by relatively short rivers. This is because they are derived from a relatively smaller catchment, and therefore might drain fewer geological lithologies. Short rivers also transport sediments from source

* **Corresponding author: Amon Kimeli,** Department of Geoscience, University of Bremen, 28359 Bremen, Germany; Biogeochemistry and Geology Department, Leibniz Centre for Tropical Marine Research (ZMT), 28359 Bremen, Germany; Oceanography and Hydrography Department, Kenya Marine and Fisheries Research Institute, 81651 – 80100 Mombasa, Kenya, e-mail: amon.kimeli@leibniz-zmt.de
**Oliver Ocholla, Judith Okello, James Kairo:** Oceanography and Hydrography Department, Kenya Marine and Fisheries Research Institute, 81651 – 80100 Mombasa, Kenya
**Nico Koedam:** Biology Department, Laboratory of Plant Biology and Nature Management (APNA), Vrije Universiteit Brussels, 1050 Brussels, Belgium
**Hildegard Westphal:** Department of Geoscience, University of Bremen, 28359 Bremen, Germany; Biogeochemistry and Geology Department, Leibniz Centre for Tropical Marine Research (ZMT), 28359 Bremen, Germany

to mouth in shorter periods of time, allowing for less alteration [6,7]. Additionally, the composition of sediments is altered by *in situ* production of bio-clasts, mostly calcareous shells, and the formation of authigenic minerals [5].

During transportation, fluvial sediments provide efficient sinks for major and trace elements to accumulate [7]. Major and trace elements are introduced into the aquatic environments (rivers, oceans, and lakes) through both natural and anthropogenic ways. The natural ways include atmospheric deposition, weathering of source geology, erosion, and surface runoffs and anthropogenic activities include mining and discharge of sewage effluents [8]. In the lowermost course of rivers such as in dynamic systems like estuaries, deltas, bays, or creeks the mixing of sediments from multiple sources alters the compositional characteristics. It therefore adds to the complexity when untangling sediment provenance using bulk mineralogical or chemical compositions in such systems.

A combination of mineralogical and chemical composition of sediments and rocks has been utilized in numerous studies to constrain source characteristics and to evaluate the degree of weathering and alteration during transportation [6,7,9]. Source characteristics include the geological and tectonic setting of the source catchments as well as paleoclimatic conditions [9,10]. To evaluate these characteristics and improve the disentangling of sediment provenance, sediments can be chemically divided into the residual initial sediment composition and the labile fractions. The residual initial composition represents the close to source characteristics, while the labile fractions represent the altered composition as a function of fluvial transportation distance and time [11]. Less mobile elements tend to be less susceptible to alteration, thus they are suitable proxies for evaluating the source area composition [3], and are used as tracers for sediment provenance. These elements include iron (Fe), vanadium (V), magnesium (Mg), thorium (Th), rare earth elements, and their ratios to aluminum (Al) [4,12]. These elements are considered immobile due to their low solubility and relative retention of their characteristics during transport, reworking, deposition, and diagenesis [4]. However, it has also been shown that dominant minerals and some large labile fractions (mostly clays, carbonates, and organic matter) can influence the chemical and mineralogical composition of sediments. Therefore, grain size can influence the chemical and mineralogical compositions of fluvial sediments mainly because some grain sizes, especially highly cohesive and consolidated clays (<125 μm), provide better element sinks than relatively unconsolidated medium-grain sand (0.25–0.5 mm) to very fine sand or silt (62.5–125 μm) [13]. Sediments with elevated sand content (up to >80%) have been reported to act generally as inert dilutors of trace elements and conducive for enhanced accumulation of some elements including Cr, Ni, and Co [13].

The provenance of coastal sediments in our study area so far has received little attention. Our main hypothesis is that the sediments deposited along the Umba River including those that are deposited in the downstream estuary, reflect faithfully the geology of the catchment that extends upstream to the Usambara mountains in southeast Tanzania. The primary purpose of our study is to characterize the geochemistry and mineralogy of the sediments along the Umba river and in the coastal area of Vanga, in order to provide information on the source characteristics, weathering, and their provenance. This study provides knowledge on this transboundary setting and thus contributes toward integrated cross-border management of common resources. Sedimentation is a vital component in this management endeavor not only because of the connectivity of the wider catchment land use but also their effects in downstream biotopes. For example, intensification of land use may increase the soil erosion and delivery of sediments to the downstream habitats, resulting in both negative and positive impacts. The positive effects would include delivery of particulate and dissolved nutrients – vital in the biogeochemical cycles, and sediments – with the accretion of sediments indirectly benefiting mangroves in response to the rising sea level. Conversely, too high input of nutrients and sediments, as well as delivery of contaminants from the hinterland, is detrimental to downstream biotopes. For example, excessive sedimentation can lead to mangrove burial and die-back, and increasing turbidity can cause damage to coral reefs and seagrass beds in the adjacent coastal areas.

## 1.1 Climate

The tropical climate of this region is influenced by the monsoon winds attributed to the proximity of the warm Indian Ocean and the north-south inter-annual migration of the Inter-Tropical Convergence Zone (ITCZ) [14,15]. This ITCZ migration and the resulting changes in wind directions coin two major seasons, namely the southeast monsoon (SEM) and the northeast monsoon (NEM). The NEM brings with it two rainy seasons, the "long rains" between March and June and the "short rains" between October and mid-December. Conversely, the SEM causes two dry seasons sandwiched between the two rainy (wet) seasons [14,16]. The mean annual precipitation in this region reaches 4,000 mm, and the average annual

temperature is at 25°C. The "long rains" account for the majority of the annual rainfall, and consequently water discharge and annual sediment transport of the Umba River [17].

# 2 Geological setting

The geology of the catchment area is dominated by the Precambrian basement, successively covered by younger lithologies toward the East (Figure 1a and 1b). A zone composed of Paleozoic to Jurassic rocks of the Karoo Supergroup (540–145 million years) stretches north-south (Figure 1a) along the East of the Tanzanian craton [18], followed by a cover of inter-layered and inter-banded Meso-zoic and Cenozoic lithostratigraphic deposits (Figure 1b). The Karoo Supergroup stretching from the Tanga basin in Tanzania to the southwest of Kenya comprises generally of sandstones, arkoses, arkosic sandstones, conglomerates, and siltstones [19]. The Precambrian (Neoproterozoic) base-ment is characterized by high-grade metamorphic gneisses, marbles, gneissic-schists, and quartzites. These were intruded by younger East African Rift basaltic extrusive igneous rocks [18,19] dominated by pyroxene-garnet granulites interlaced with hornblende-gneiss lithologies.

The upper reaches of the Umba River in the Usambara mountains consist of thick sequences of granulite facies ortho-gneisses (625 Ma) derived from andesitic to dacitic magmatism in a convergent margin [18,20]. This formation is intercalated with pelitic, calc-argillaceous, and calcar-eous meta-sediments [18,21,22]. The meta-igneous rocks are also intruded by mafic and felsic bands of gabbro, anortho-site, and hornblende/pyroxenite facies. The quartzo-felds-pathic and hornblende-pyroxene granulites are character-ized by varying portions of quartz, K-feldspars, plagioclase, hornblende, pyroxenes, biotite, and magnetite and acces-sorized by apatite, ilmenite, and zircon [18,21,23]. Close to the source of the Umba River in Usambara mountains, the Precambrian basement and the associated lithologies are highly weathered and degraded at the surface, forming red-dish-brown soils.

Further downstream, warping along the eastern border of the Precambrian, toward our study site in both Kenya and Tanzania, Paleozoic rocks crop out, mainly belonging to the Karoo Supergroup. Here due to extensive agriculture and transition to sedimentary and meta-sedimentary rock lithol-ogies, the soils exhibit a dark-brown coloration [18,20]. Close to the coast, the Umba River crosses Quaternary sedi-ments (Figure 1b) composed mainly of quartz and calc-sili-cate minerals [19,25].

## 2.1 Study site

The Umba River originates in the tectonically uplifted Usambara Mountains in Mkinga, Tanzania, with an ele-vation of *circa* 2,000 m above mean sea level, and drains to the Indian Ocean in Vanga, Kenya (Figure 2). The man-groves of Vanga at the south coast of Kenya (Figure 2) receive the terrigenous sediments from the relatively short *circa* 200 km long Umba River. It drains a catch-ment of *circa* 8,000 km² [17]. Part of the study area lies within a proposed Transboundary Conservation Area (TBCA) between Kenya and Tanzania (Figure 2), which extends south from Diani within the Kwale County in Kenya (39°00′ E, 4°25′ S) to Tanga within the Mkinga District in Tanzania (39°40′ E, 5°10′ S) covering a north-south distance of *circa* 120 km and a narrow strip along the coastline in Kenya and Tanzania, with an estimated total area of *circa* 2,500 km². The TBCA intends to integrate and align the coastal conserva-tion and management in an ecologically connected region transcending the Kenya–Tanzania border. The proposed TBCA will have significant ecological significance mainly because it is characterized by contiguous and connected marine and terrestrial habitats as well as similar and shared socio-economic status [15]. Sampling for the pre-sent study was done at seven stations along the Umba River from source to mouth. Stations S1, S2, and S4 are located on the Tanzanian side, while Stations S5, S6, S7, and S8 are on the Kenyan side (Figure 2).

# 3 Materials and samples

Riverbank (*n* = 32) and bottom sediment (*n* = 26) samples were collected from the Umba River in Tanzania and Kenya during the transition period between the dry and the rainy seasons (June–July 2019). The sediment sam-ples were collected along the course of the river at five upstream riverine stations (S1, S2, S4, S5, and S6), one downstream estuarine station (S7), and one marine sta-tion in the river mouth (S8). Riverbank samples were collected on either sides of the river above the waterline, while the bottom samples were taken – where acces-sible – in the middle of the river channel. All samples collected at stations S7 and S8 were considered as bottom sediments due to the daily inundation by flood tides. Riverbank sediments were collected using a pre-cleaned hand-held shovel, while the estuarine and marine sedi-ments were sampled using a hand-held Van Veen grab sampler at water depths between 5 and 10 m. The sedi-ment samples were assumed to have been recently
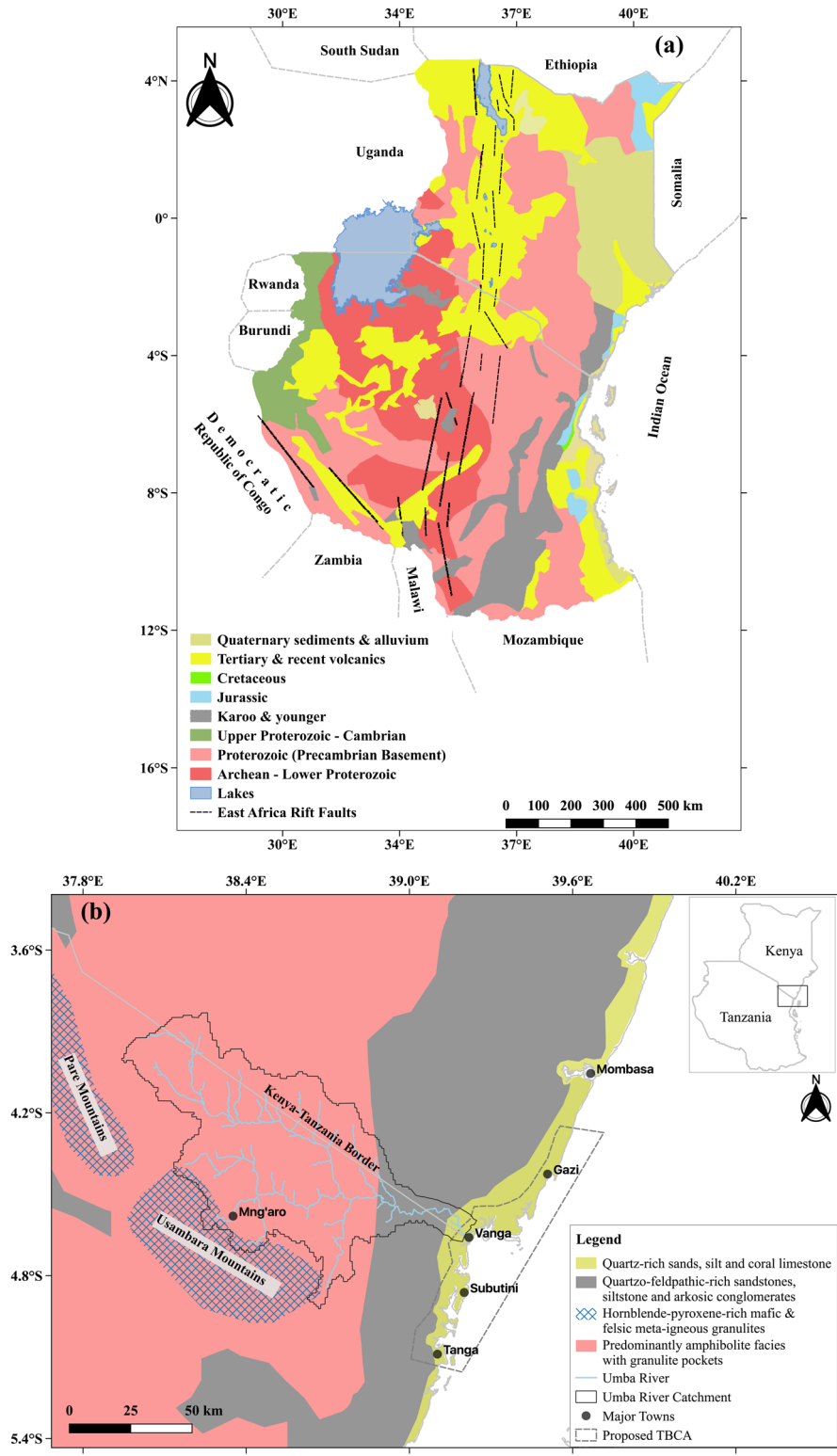
**Figure 1:** Map showing the regional geology and the key stratigraphic units (a) and the general geology and the dominant lithologies of the Umba River catchment from its upper reaches in Mng'aro, Tanzania to the river mouth in Vanga, Kenya in the lower reaches (b). Inset is a map of Kenya and Tanzania (b). Maps are modified from refs [18,19,24].
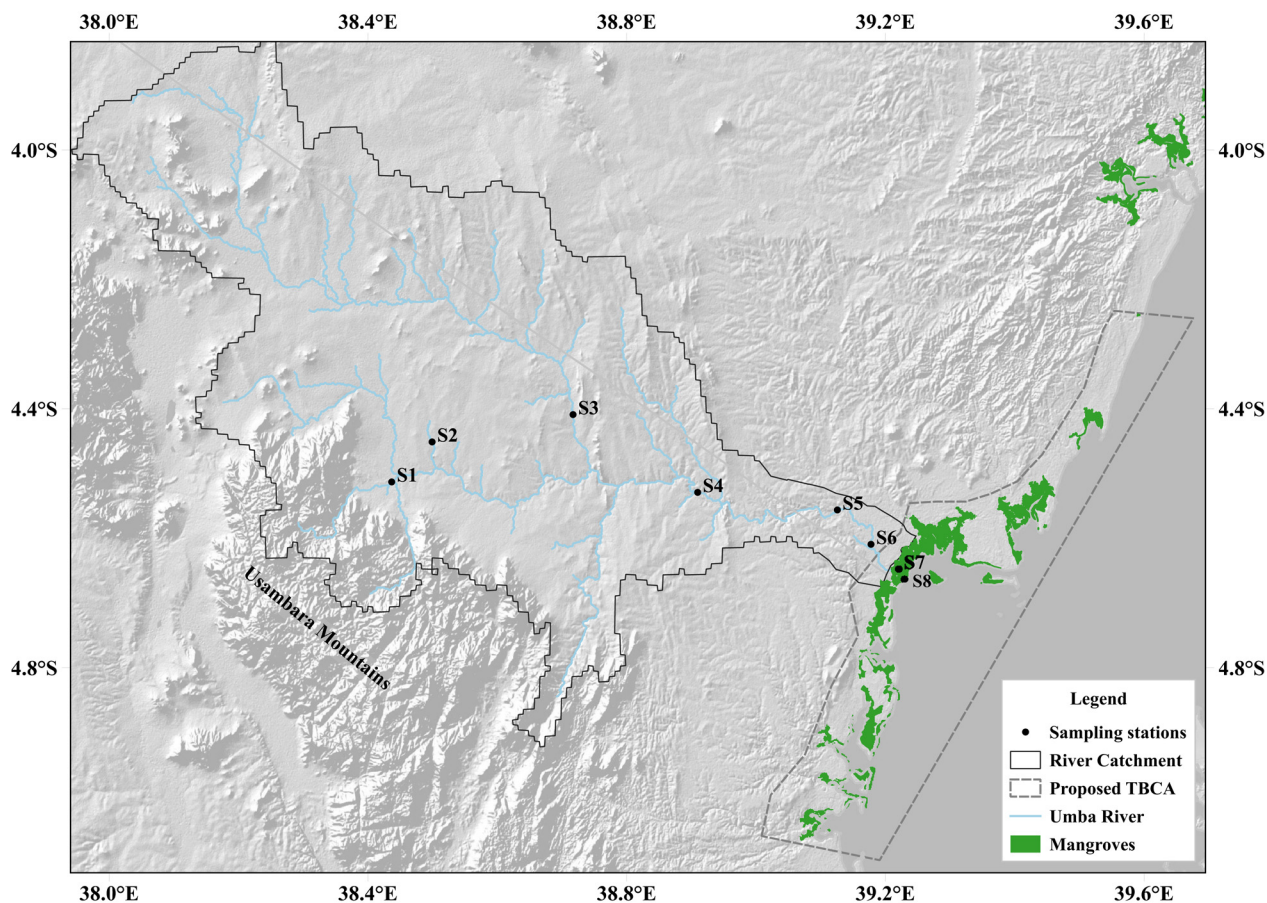
**Figure 2:** The study site within the Umba River catchment and sampling locations along the Umba River. Stations S1, S2, S3, and S4 in Tanzania and S5, S6, S7, and S8 in Kenya.

deposited, without significant post-depositional reworking. Three replicates of the sediment samples in each station were collected and placed in sealed plastic bags for transporting to the lab. Aliquots of the sampled sediments were obtained for petrographic, grain size, and geochemical analyses.

## 3.1 Grain size analysis

Grain size analysis of the bulk river sediment samples was conducted in a laboratory at the Kenya Marine and Fisheries Research Institute, Kenya, using a Malvern© Mastersizer 2000 laser diffraction particle size analyzer. Sediment pre-analysis treatment including removal of organic matter using 30% of hydrogen peroxide and clastic grains >2 mm [26] was undertaken before measurement of grain sizes according to Hossain et al. [26]. Mean grain size (µm) was estimated according to Folk and Ward [27].

## 3.2 Petrographic analysis

Thin sections were prepared at the geology laboratory of Leibniz Centre for Tropical Marine Research (ZMT), Germany, according to protocols in refs [28,29]. Small blocks (4 cm × 4 cm) of dried sediment samples were bound together with Araldite 20/20 resin. The blocks were hardened and after 24 h, one side of the block was ground to obtain a plain surface without scratches. The plain surface was cleaned in an ultrasonic bath and dried. The dried block was fixed with resin on a glass slide and bound together using a press system. Once it was bound together and hard-dried again for another 24 h, the block was cut into 1 mm slices and polished parallel to the glass slide to obtain one single thin section. The 1 mm sample was then ground on the slide down to 100 µm and further ground to 28 µm suitable for mineralogical analyses. The thin sections were examined under an optical polarized light in LEICA DM500-EP microscope.

## 3.3 Major and trace elements

In the laboratory, wet sediment samples were dried at 60°C for 48–72 h, pulverized and homogenized using a Fritsch© Planetary Micro ball-mill Pulverisette 7. Seven hundred milligram of each sample was mixed with 4,200 mg of di-Lithium tetraborate (Spectro-melt A10, $B_4Li_2O_7$) and pre-oxidized with 1,000 mg of ammonium nitrate at 500°C. The sample mixtures were then digested (melted) at 1,340–1,350°C in a CIMREX$^{TM}$ 10 microwave accelerated reaction system, using a combination of HF + HNO$_3$ + H$_3$BO$_3$ for major and trace element analyses [30–32] and then fused to homogeneous glass pellets (beads). The pellets were then analyzed in PANalytical© AXIO Max (3 kW) by wavelength-dispersive X-ray fluorescence. Major elements (as oxides) were reported in wt%, while the trace elements were given in ppm [33]. The accuracy of the analytical procedures was verified by analyzing three certified standard reference materials namely PACS, MESS, and PS-S. The major elements measured included Si, Ti, Al, Fe, Mn, Mg, Ca, K, Na, and P. The oxides of major elements were also used to constrain and assign the sediment provenance using first and second discriminant functions (DF1 and DF2) analysis [9,34,35]. Large-ion lithophile elements including Rb, Ba, Sr, Th, U, and Ce were measured. The high field strength elements including Zr, Y, and Nb were also measured, as were the transition trace elements, i.e., Cr, Co, Cu, Ni, Zn, Ga, Mo, and Pb.

## 3.4 Degree of weathering and chemical alteration

Several weathering indices are available to evaluate mineralogical maturity, chemical alteration, and element mobility [34,36–38]. The underlying principle of weathering indices is the comparison of mobile elements with immobile elements such as Al as the ref. [39]. Such immobile elements are less susceptible to alteration and weathering. They, therefore, retain their chemical characteristics over longer periods and longer distances of transportation by rivers. In this study, the chemical index of alteration (CIA) was used to evaluate the degree of feldspar alteration, calculated using the equation [40]:

$$CIA = [Al_2O_3/(Al_2O_3 + CaO^\star + Na_2O + K_2O) \times 100].$$

The CIA is represented in molecular proportions, where CaO$^\star$ represents the Ca in silicate fraction only, adjusted for other Ca-bearing minerals such as carbonates [41]. The abundances of the major elements were used to

evaluate the chemical composition and provenance of Umba River sediments following the rationale described in refs [6,34,39]. To further evaluate the effect of transport and weathering, ternary plots were generated from the major element compositions of Umba River sediments [40]. Specifically, ternary plots were created showing the concentration on $Al_2O_3 - (CaO + Na_2O) - K_2O$, hereafter referred to as A-CN-K, and $Al_2O_3 - (CaO + Na_2O + K_2O) - (Fe_2O_3 + MgO)$, hereafter referred to as A-CNK-FM. The position of sediments within the ternary diagrams indicates the dominant minerals, degree of weathering, mineral sorting, and thereby, the source geology. Specifically, A-CN-K and A-CNK-FM plots assist in the understanding of feldspar weathering and the effects of sorting on weathering of Fe-Mg bearing minerals, respectively [6,34].

## 3.5 Provenance

The compositional data of the Umba River sediments were also used to constrain their sedimentary provenance. Discriminant function plots express oxides of various elements as ratios with the immobile $Al_2O_3$ [34]. DF analysis based on oxide ratios distinguishes the provenance of sediments between four fields, namely mafic igneous, felsic igneous, intermediate igneous, and quartzose (recycled) sedimentary provenance [26,34]. DF analyses based on raw oxides are represented by the following equations;

Discriminant Function (DF1)
$$= (30.638TiO_2/Al_2O_3) - (12.541Fe_2O_3/Al_2O_3)$$
$$+ (7.329MgO/Al_2O_3) + (12.031Na_2O/Al_2O_3)$$
$$+ (35.402K_2O/Al_2O_3) - 6.382,$$

Discriminant Function (DF1)
$$= (56.500\ TiO_2/Al_2O_3) - (10.879Fe_2O_3/Al_2O_3)$$
$$+ (30.875MgO/Al_2O_3) - (5.404Na_2O/Al_2O_3)$$
$$+ (11.112K_2O/Al_2O_3) - 3.89.$$

## 3.6 Statistical analyses

Statistical analyses were performed using inbuilt R-program (v. 1.1.463) libraries and packages (R Core Team, 2020). Significant difference tests of major and trace element concentrations between sediment type (riverbank or bottom sediments) and environment (riverine, estuarine, and marine) were assessed by performing an analysis of

variance (ANOVA). Data conformity to normal distribution was examined using the Shapiro–Wilk test of normality.

# 4 Results

Mean concentrations of major and trace elements of the Umba River sediments are presented in Table 1 and the primary dataset in the Supplementary Information 1. Detailed results of the statistical analyses are summarized in Supplementary Information 2. From the performed statistical analysis, some oxides and trace elements showed significant variability ($p < 0.05$) between the sediment types (riverbank and bottom sediment), and some among environments (riverine, estuarine, and marine) (Supplementary Information 2). Despite the significant difference, both the riverbank and bottom sediments showed similar distribution trends from source to mouth.

## 4.1 Grain size distribution

The Umba River sediments are composed of sand, silt, and clay in different proportions (Table 1; Figure 3). The mean grain size (μm) of the riverbank and bottom sediments is 172 and 266 μm, respectively (Table 1). The mean dominant fractions are sand and silt, ranging between 34 and 78% and 0.72 and 62% of total volume percentages, respectively. Clay constitutes less than 3% in both the riverbank and bottom sediments with an overall range between 0.07 and 2.90%. The grain size gradient is typical for rivers and transitions from predominantly coarse sandy sediments in the upper catchment (S1, S2, S4, S5, and S6) to sandy-silt-sized with clay in the estuary (S7) and silty-sand-sized sediment at the marine site (S8) (Figure 3 and Table 1). Clay-sized particles were most abundant in the estuarine stations (S7) compared to all the other stations.

## 4.2 Mineralogy of Umba River sediments

The mineralogical composition identified by petrographic analyses is similar for the upstream riverine sediments and the downstream estuarine and marine sediments (Figures 4 and 5). All sediments along the entire course of the Umba River (Figure 2) contain mainly K-feldspar, lamellar and striated plagioclase, quartz, muscovite, biotite, and hornblende. Accessory minerals include opaque and clay minerals that were not further identified here. However, from comparison of site-relevant literature [18,20], we infer that the opaque minerals include magnetite, ilmenite, and maghemite. Additionally, clay minerals such as kaolinite and illite are also reported for the Umba River catchment.

The quartz crystals occur as elongated and deformed lenticular grains. They are also present in lithoclasts, where they exhibit anhedral shapes adjacent and surrounding feldspar, biotite, and other minerals. In the lithoclasts, the feldspars (K-feldspars and plagioclase) exhibit tabular and irregular crystals [42]. The sediments collected in the downstream stations (S7 and S8) show evidence of river transportation or high energy environments, characteristic of intertidal areas due to their relatively rounded shapes (Figure 5). From source to mouth, a decrease in lithoclast sizes is observed that goes along with an increase in the monocrystalline grains (as opposed to lithoclasts made up of multiple crystals) (Figures 4 and 5). Downstream sediments (Figure 5) exhibit poor grain sorting and varying degrees of roundness of the individual clasts.

## 4.3 Major elements

The sediments exhibit a relatively narrow $SiO_2$ range in both the riverbank sediments (53.30–70.43 wt%, with an average of 59.89 wt%) and bottom sediments (55.57–76.22 wt%, with an average of 65.76 wt%) (Table 1). Highest $SiO_2$ contents coincide with coarse-grained sediments, for example, in station S4 for riverbank and S8 for bottom sediments. Low $SiO_2$ content (55.67 wt%) is observed in the estuarine silty sands collected in station S7 (Table 1). The $Al_2O_3$ content varies between 10.45 and 19.06 wt% (average of 15.97 wt%) in riverbank sediments, and between 9.90 and 17.12 wt% (average of 13.64 wt%) for bottom sediments (Table 1 and Supplementary Information 1). $Fe_2O_3$ and $TiO_2$ contents were >5 wt% and <2 wt%, respectively, in both the riverbank and bottom sediments. The immobile $Al_2O_3$ shows a clear negative relation with $SiO_2$ in both the riverbank and bottom sediments (Figure 6a). There is no particular trend on $Al_2O_3$ versus $TiO_2$ in riverbank sediments but a positive relation in the bottom sediments (Figure 6b). $Al_2O_3$ also shows a positive relation with $Fe_2O_3$ and $P_2O_5$ in both the riverbank and bottom sediments (Figure 6c and d).

The alkaline oxides, i.e., $K_2O$, $Na_2O$, and $MgO$, are relatively high (>1 wt%) in all stations and in both riverbank and bottom sediments (Table 1; Supplementary Information 1). However, on average $K_2O$ and $MgO$ are slightly higher in riverbank sediments compared to bottom sediments (1.46 and 1.68 wt%, respectively). $Na_2O$ content is highest (2.14 wt%) in bottom sediments (Table 1). Additionally, the total alkali content ($K_2O + Na_2O$) and the alkali ratios ($K_2O/Na_2O$) in all the stations are >2.5 and >0.5%, respectively, in both the riverbank and bottom

**Table 1:** Grain size distribution (in µm), major element (in wt%), and trace element (in ppm) contents in riverbank and bottom sediments of Umba River

| Sample station | Riverbank sediments | | | | | Bottom sediments | | | | |
|---|---|---|---|---|---|---|---|---|---|---|
| | **S1** | **S2** | **S4** | **S5** | **S6** | **S1** | **S2** | **S4** | **S7** | **S8** |
| Grain size distribution | | | | | | | | | | |
| Mean grain size (µm) | 160.36 | 90.44 | 394.14 | 109.88 | 106.37 | 90.41 | 141.41 | 861.41 | 72.49 | 166.32 |
| Sorting ($\sigma_g$) | 3.87 | 3.32 | 3.04 | 3.58 | 4.92 | 3.58 | 3.56 | 1.75 | 4.03 | 2.57 |
| Skewness ($Sk_g$) | −0.23 | −0.27 | −0.25 | −0.25 | −0.28 | −0.14 | −0.18 | −0.13 | 0.08 | 0.01 |
| Kurtosis ($K_g$) | 0.80 | 1.06 | 1.28 | 1.06 | 0.92 | 0.95 | 1.05 | 0.93 | 0.98 | 0.89 |
| Sand (%) | 60.78 | 63.75 | 67.04 | 58.51 | 57.79 | 59.12 | 70.94 | 65.69 | 34.23 | 78.83 |
| Silt (%) | 33.43 | 34.84 | 16.98 | 39.04 | 37.06 | 39.21 | 25.86 | 0.72 | 62.08 | 20.14 |
| Clay (%) | 0.22 | 1.41 | 0.07 | 1.75 | 2.06 | 0.72 | 0.81 | 0.07 | 2.90 | 1.03 |
| Major elements (wt%) | | | | | | | | | | |
| $SiO_2$ | 57.05 | 56.26 | 70.43 | 62.39 | 53.30 | 61.70 | 63.75 | 76.22 | 55.67 | 71.47 |
| $TiO_2$ | 1.12 | 0.82 | 1.76 | 1.45 | 0.90 | 0.97 | 1.04 | 0.73 | 0.80 | 0.70 |
| $Al_2O_3$ | 16.50 | 18.50 | 10.45 | 15.33 | 19.06 | 15.43 | 14.60 | 9.90 | 17.12 | 11.18 |
| $Fe_2O_3$ | 8.50 | 7.27 | 7.48 | 7.25 | 8.36 | 8.17 | 7.72 | 4.30 | 7.61 | 3.95 |
| MnO | 0.23 | 0.12 | 0.12 | 0.13 | 0.15 | 0.18 | 0.15 | 0.07 | 0.12 | 0.09 |
| MgO | 1.84 | 1.71 | 1.72 | 1.71 | 1.40 | 1.81 | 1.81 | 1.42 | 1.52 | 1.50 |
| CaO | 4.04 | 3.61 | 2.65 | 2.90 | 1.88 | 3.25 | 3.47 | 2.44 | 1.52 | 4.45 |
| $Na_2O$ | 1.92 | 2.26 | 1.59 | 2.14 | 1.21 | 2.12 | 2.21 | 1.75 | 1.88 | 2.75 |
| $K_2O$ | 1.23 | 1.50 | 1.40 | 1.66 | 1.48 | 1.12 | 1.34 | 1.58 | 1.39 | 1.53 |
| $P_2O_5$ | 0.11 | 0.18 | 0.09 | 0.14 | 0.24 | 0.17 | 0.13 | 0.08 | 0.21 | 0.10 |
| $SO_3$ | 0.01 | 0.02 | 0.02 | 0.03 | 0.02 | 0.00 | 0.01 | 0.01 | 0.13 | 0.04 |
| LOI | 7.01 | 7.56 | 2.04 | 4.60 | 11.79 | 4.91 | 3.60 | 1.26 | 11.86 | 2.04 |
| Total | 99.56 | 99.79 | 99.74 | 99.72 | 99.78 | 99.82 | 99.81 | 99.76 | 99.83 | 99.80 |
| CIA | 58.43 | 60.83 | 53.98 | 58.91 | 73.13 | 59.16 | 56.20 | 52.04 | 68.01 | 44.50 |
| ICV | 1.18 | 0.95 | 1.63 | 1.17 | 0.81 | 1.15 | 1.22 | 1.25 | 0.91 | 1.35 |
| $K_2O + Na_2O$ | 3.15 | 3.76 | 2.99 | 3.81 | 2.68 | 3.24 | 3.54 | 3.33 | 3.27 | 4.28 |
| $K_2O/Na_2O$ | 0.73 | 0.69 | 0.92 | 0.81 | 1.37 | 0.53 | 0.61 | 0.93 | 0.77 | 0.56 |
| $Al_2O_3/SiO_2$ | 0.30 | 0.34 | 0.15 | 0.25 | 0.37 | 0.25 | 0.23 | 0.13 | 0.34 | 0.16 |
| $Fe_2O_3/SiO_2$ | 0.15 | 0.13 | 0.11 | 0.12 | 0.16 | 0.13 | 0.12 | 0.06 | 0.15 | 0.06 |
| Trace elements (ppm) | | | | | | | | | | |
| Ce | 51.33 | 46.00 | 86.17 | 76.50 | 70.60 | 47.00 | 47.67 | 32.33 | 55.53 | 34.00 |
| Co | 20.22 | 16.67 | 13.17 | 16.17 | 23.20 | 16.50 | 14.67 | 10.00 | 16.47 | 8.67 |
| Cr | 70.67 | 45.83 | 236.67 | 92.83 | 92.00 | 61.50 | 45.67 | 133.33 | 80.87 | 51.33 |
| Cu | 53.44 | 51.50 | 13.33 | 28.33 | 69.00 | 36.00 | 29.00 | 8.00 | 51.07 | 5.00 |
| Ga | 16.33 | 17.33 | 9.00 | 14.50 | 19.60 | 15.50 | 13.00 | 8.67 | 17.13 | 8.67 |
| Mo | 2.00 | 1.17 | 2.00 | 1.67 | 1.60 | 1.50 | 1.67 | 2.33 | 3.07 | 1.67 |
| Nb | 12.67 | 9.83 | 17.67 | 18.00 | 14.20 | 10.00 | 12.00 | 8.67 | 12.07 | 9.00 |
| Ni | 28.89 | 22.00 | 43.67 | 30.00 | 48.40 | 24.50 | 17.00 | 34.33 | 38.47 | 10.00 |
| Pb | 7.78 | 6.33 | 5.83 | 10.50 | 11.40 | 6.50 | 4.33 | 6.00 | 9.53 | 6.67 |
| Ba | 1004.6 | 1034.2 | 842.33 | 1065.33 | 898.40 | 803.50 | 895.67 | 959.33 | 635.33 | 974.00 |
| Rb | 34.44 | 35.67 | 29.50 | 45.00 | 60.00 | 28.50 | 27.67 | 31.67 | 55.00 | 28.67 |
| Sr | 350.00 | 438.17 | 300.17 | 382.83 | 263.20 | 333.50 | 387.33 | 329.67 | 232.80 | 472.67 |
| Th | 4.56 | 4.00 | 11.17 | 6.83 | 6.00 | 4.50 | 3.67 | 4.00 | 6.13 | 3.67 |
| U | −0.67 | −1.00 | −0.33 | −0.33 | −0.60 | −0.50 | −1.33 | −0.33 | 0.80 | 0.33 |
| V | 168.67 | 147.67 | 183.83 | 166.17 | 161.00 | 153.00 | 167.33 | 98.00 | 141.20 | 81.67 |
| Y | 19.44 | 17.00 | 20.33 | 21.67 | 23.80 | 17.00 | 20.67 | 11.67 | 19.33 | 13.00 |
| Zn | 105.22 | 74.83 | 53.67 | 70.33 | 89.20 | 87.50 | 64.33 | 34.00 | 74.60 | 39.67 |
| Zr | 258.78 | 184.83 | 541.00 | 417.50 | 169.80 | 238.00 | 266.33 | 349.33 | 255.27 | 291.33 |
| Cr/Ni | 2.63 | 2.15 | 3.54 | 3.71 | 1.96 | 2.55 | 2.77 | 3.99 | 2.51 | 5.11 |
| Rb/Sr | 0.10 | 0.08 | 0.10 | 0.12 | 0.26 | 0.09 | 0.07 | 0.10 | 0.24 | 0.06 |
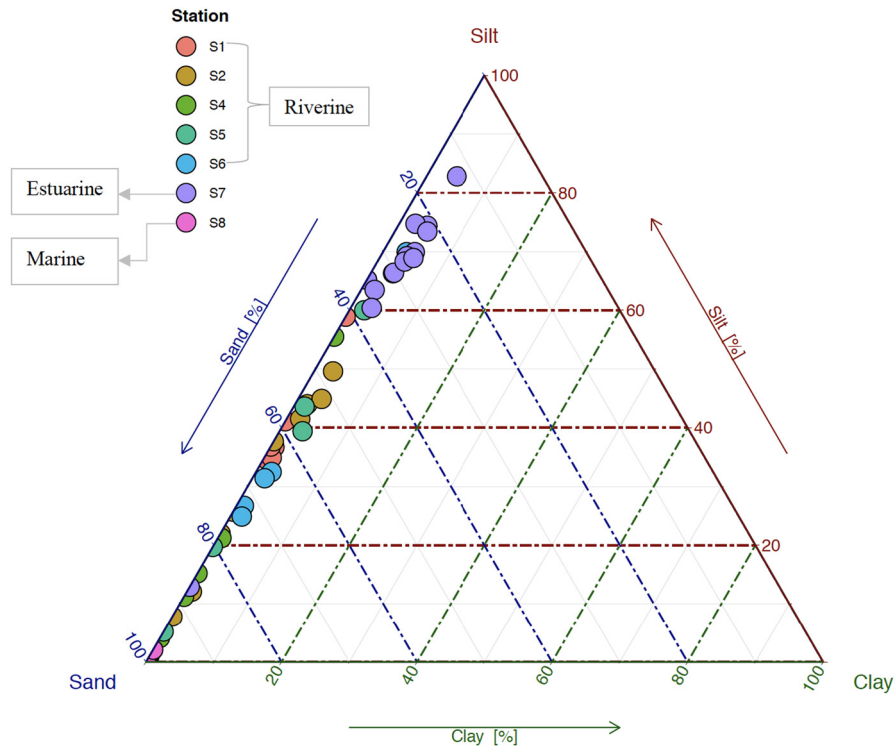
**Figure 3:** Ternary diagram showing textural distribution of sediments during the transition period (July 2019). With S1–S6 being upstream riverine stations and S7 and S8 being downstream estuarine and marine stations, respectively.
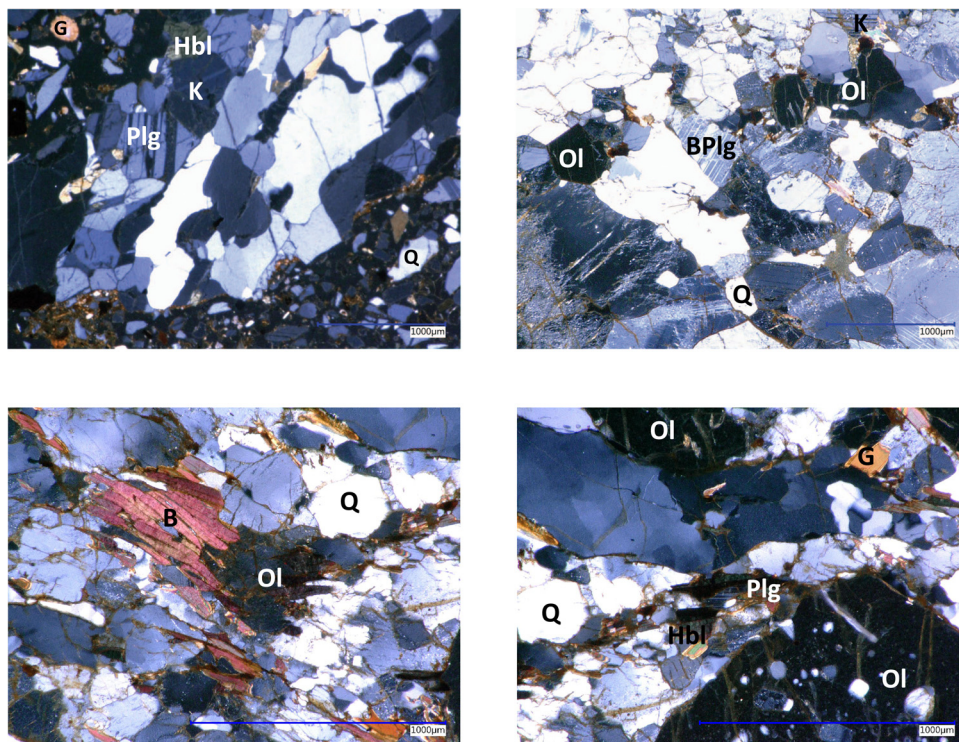


**Figure 4:** Photomicrographs of individual lithoclasts in upstream sediments (left to right: stations S1 and S4 (top row) and stations S5 and S6 (bottom row)). K = K-feldspar, BPlg = Banded plagioclase, G = Garnet, Q = Quartz, Hbl = Hornblende, B = Biotite, and Ol = Olivine.
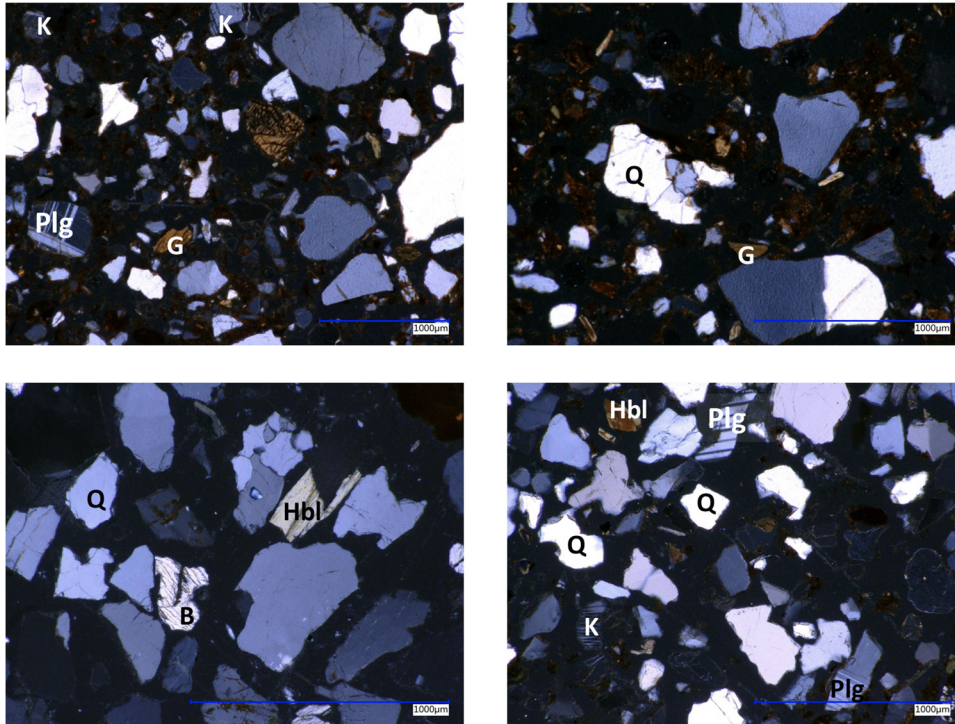
**Figure 5:** Photomicrographs of individual mineral lithoclasts in downstream sediments embedded in epoxy resin. Top row S7 (estuary) and bottom row S8 (marine setting). K = K-Feldspar, Plg = Banded plagioclase, G = Garnet, Q = Quartz, Hbl = Hornblende, and B = Biotite.

sediments (Table 1). The sediments exhibit a wide range of CaO values in riverbank (1.88–4.04 wt%, average of 3.01 wt%) and in bottom sediments (1.52–4.45 wt%, average of 3.03 wt%) (Table 1). A negative relation between $Al_2O_3$ and CaO (Figure 6e) and $K_2O$ (Figure 6f) is observed in the riverbank as well as in the bottom sediments. Additionally, CaO is relatively depleted in estuarine sediments (S7) compared to riverine and marine sediments. Both MgO and $N_2O$ show a positive but scattered relation with the immobile $Al_2O_3$ (Figure 6g and h, respectively). Major element ratio $Al_2O_3/SiO_2$ vs $Fe_2O_3/SiO_2$ exhibits a wide variation in all the grain size fractions and covers the entire quartz–clay spectrum (Figure 7). The larger grain size fractions (e.g., S4, S6, and S8) show similar enrichment of Fe and Al, as exhibited by the fine fraction and relatively clay-rich estuarine sediments (S7).

## 4.4 Trace elements

Average concentrations of the trace elements Cr, Ni, and Zn are all enriched in riverbank sediments compared to bottom sediments (Table 1, Supplementary Information 1). Cr concentration ranges between 25 and 346 ppm with an average of 107.60 and 34.59 ppm in riverbank and bottom sediments, respectively. Ni concentration ranges between 5 and 73, again showing a higher average of

34.59 ppm in riverbank sediments compared to bottom sediments (24.86 ppm) (Table 1; Supplementary Information 1). Cr and Ni concentrations are depleted in marine bottom sediments collected in station S8 (Table 1). Zr concentration shows values ranging between 169 and 541 ppm (average value of 314 ppm) for river bank sediments compared to bottom sediments that show slightly lower values ranging between 238 and 349 ppm (average of 280 ppm) (Table 1). On the contrary, Sr concentration is enriched in marine (472 ppm) and riverine sediments (majority >300 ppm) (Table 1), while they are depleted in bottom estuarine sediments (232.80 ppm). The Ba content is slightly enriched in both riverbank and bottom sediments (majority >800 ppm), while the lowest Ba content of 635.33 ppm is recorded in estuarine bottom sediments (Table 1). The Rb/Sr ratios are similarly low (<0.5) in all the stations and in both the riverbank and bottom sediments, ranging between 0.06 and 0.26 with average values of 0.13 and 0.11 in the riverbank and bottom sediments, respectively (Table 1). Such low Rb/Sr ratios indicate low to moderate chemical weathering.

A less distinct and scattered relation is observed between $Al_2O_3$ and Sr (Figure 8a), while Al2O3 vs Zr shows a distinct negative relation (Figure 8b) in both the riverbank and bottom sediments. On the contrary, strong positive relations are observed between $Al_2O_3$
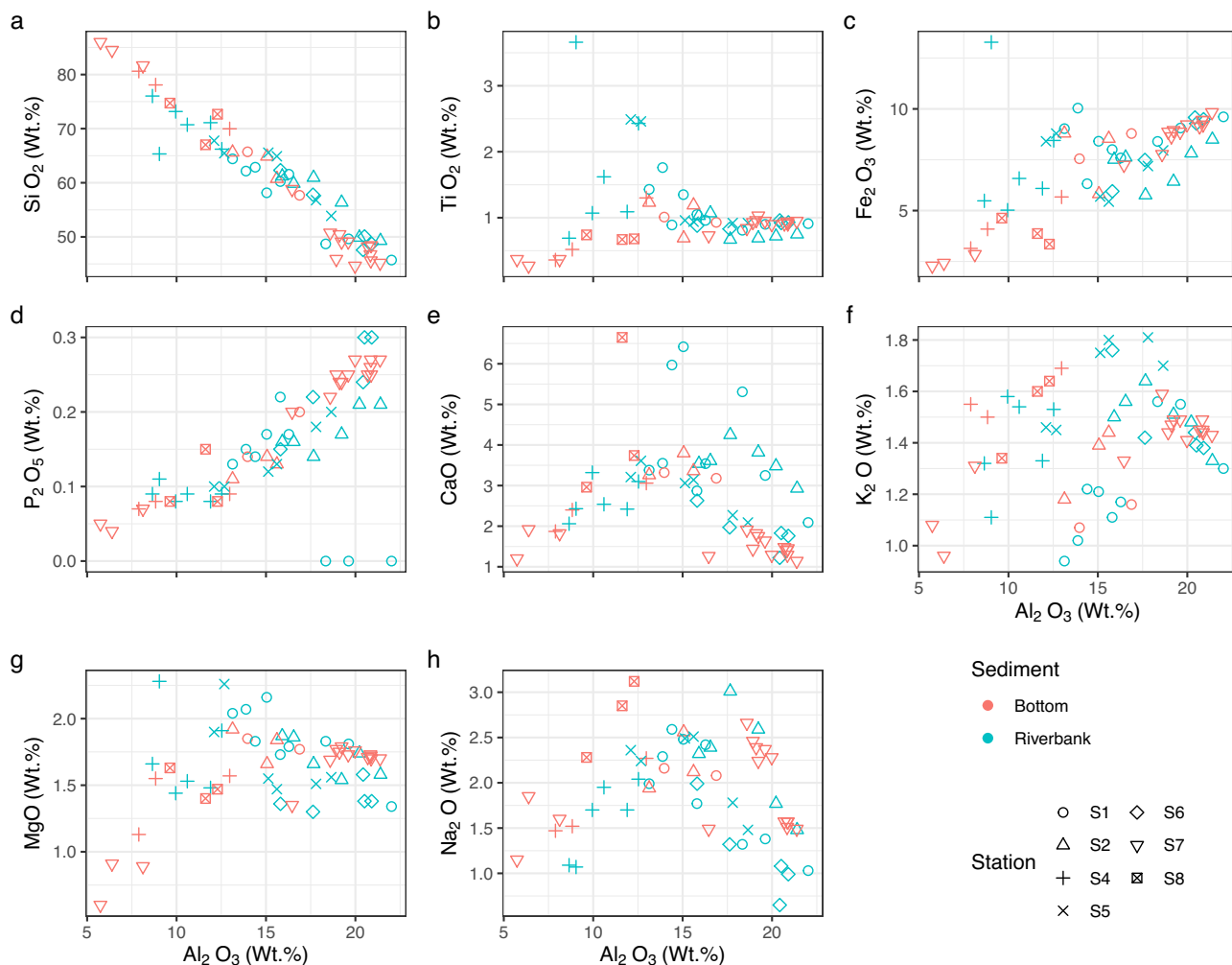
**Figure 6:** Major oxides (wt%) plots (a) $SiO_2$, (b) $TiO_2$, (c) $Fe_2O_3$, (d) $P_2O_5$, (e) CaO, (f) $K_2O$, (g) MgO and (h) $Na_2O$ for the Umba River riverbank and bottom sediments referenced to the immobile $Al_2O_3$. Strong relations are observed between the abundances of $SiO_2$ (negative), $Fe_2O_3$ (positive), and $P_2O_5$ (positive) with $Al_2O_3$ (a, c, and d respectively).

and the immobile elements Ni, Zn, Cr, and Rb (Figure 8c, d, e, and f, respectively). Relatively high positive relations are also observed between Sr and CaO as well as between the immobile Ba and $K_2O$ (Figure 8g and h, respectively) in both the riverbank and bottom sediments. Generally, a low concentration of Sr and Ba in the bottom sediments collected in the estuarine station S7 is evident (Figure 8a, g, and h).

## 4.5 Elemental ratios and weathering indices

The major and trace elements were normalized to the upper continental crust (UCC) using values from Rudnick and Gao [43]. The relative averages of the major elements show similarity with UCC values; however, the relative $Na_2O$, $K_2O$, and MgO (<0.70) concentrations are generally low compared to UCC and relative to the immobile $Al_2O_3$

(Figure 9a). Additionally, $SiO_2$ shows a marked similarity with UCC with no discernible enrichment. The average trace element compositions of the sediments show a variability that is quite comparable to other documented values from the same region [18,20]. The general pattern shows a strong depletion in Rb relative to Ba, and depletion of Th and U relative to Sr (Figure 9b).

The average UCC has a CIA value of 50, and weathered residual clay has a CIA value close to 100 [43,44]. The CIA of the Umba River sediments show a wide range, with CIA values ranging between 39 and 81 (Figure 10 and Supplementary Information 1). Within this range, the mean CIA values are higher in riverbank sediments ranging between 53.98 and 73.13 compared to the bottom sediments with values ranging between 52.04 and 68.01 (Table 1). The marine bottom sediments (collected in station S8) have the lowest CIA (Figure 10 and Table 1). The
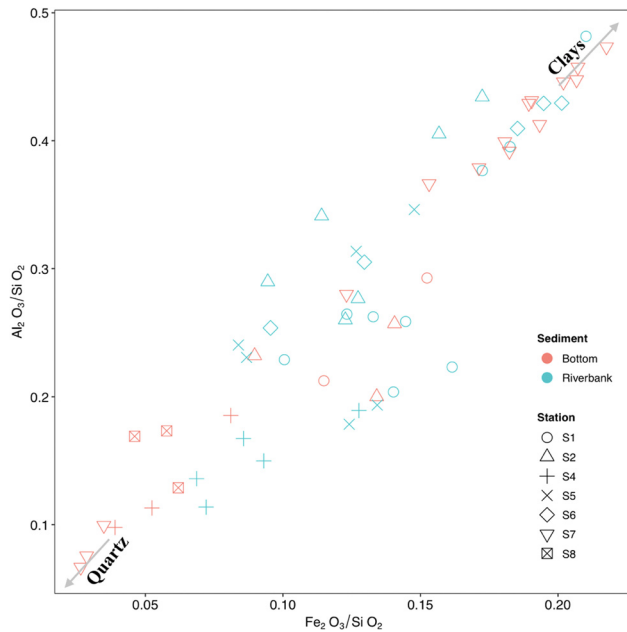
**Figure 7:** Variation in $Al_2O_3/SiO_2$ vs $Fe_2O_3/SiO_2$ ratios in Umba River sediments showing the distribution of Fe and Al elements in estuarine mud/silt sediment collected in station S7 across the entire quartz-clay spectrum.

riverbank as well as the bottom river sediments show a positive relation between CIA and $Al_2O_3$ and $Fe_2O_3$ ≥50 (Figure 10a and b). They also show elevated $Al_2O_3$, $Fe_2O_3$, and $TiO_2$ at higher CIA values of >70, while in contrast the bottom marine sediments have lower $Al_2O_3$, $Fe_2O_3$, and $TiO_2$ at CIA values of <50 (Figure 10a, b, and c). The bottom marine sediments are $K_2O$-enriched compared to the bottom estuarine sediments; however, the riverine riverbank sediments exhibited a scattered non-distinct variation at varying CIAs (Figure 10d). There is also a strong relation between Cr concentration and CIA values in the Umba River sediments especially for downstream (estuarine and marine) bottom sediments (Figure 10e).

On the A-CN-K plot, the sediments are plotted across the plagioclase – K-feldspar field (Figure 11a), while also maintaining a linear trend parallel to the A-CN edge towards the smectite field. The trendline also starts at the pristine CIA value of ~40 to a highly weathered value of ~80. The sediments are plotted below the smectite and K-feldspar field and around the K-feldspar – chlorite and K-feldspar – biotite boundaries in the A-CNK-FM (Figure 11b) with a discernible trend away from the CNK-FM boundary.

Based on the calculated DF1 and DF2, the Umba River sediments are plotted across three provenance fields, i.e., mafic igneous, intermediate igneous, and quartzose sedimentary provenance fields (Figure 12). The majority of the sediments are plotted within the mafic igneous

provenance field, which is consistent with the geology of the catchment and the associated dominant minerals.

# 5 Discussion

## 5.1 Influence of hydrodynamic and sedimentary sorting

Sediment sorting during fluvial transport, settling, and deposition can influence the mineral and chemical compositions of the sediments. Therefore, the influence of grain size sorting on sedimentary chemical composition has to be evaluated prior to any provenance determination [6,26,44,46]. For example, major and trace elements, including Al, Fe, Mg, Ni, and Cr, are known to be abundant in fine fractions of sediments rich in silt and clays, while Si is abundant in sand fractions [47,48]. In the Umba River sediments, grain sizes are distributed within a relatively narrow range between coarse sand (riverine), silty sand (marine), and sandy silt (estuarine) (Table 1; Figure 3). With minimal clay content of <3% in both the riverbank and bottom sediments, these sediments fall within the broad class of sandy sediments (Table 1). The index of compositional variability (ICV) – which is used to indicate maturity of sediments – is >1 in all riverbank and bottom sediments (Table 1). Clay minerals have been shown to exhibit an ICV <0.8 [26]. Therefore, the ICV values derived here for Umba River sediments are consistent with the observation of a very low clay fraction (Table 1). Therefore, the effects of granulometric fractions and hydrodynamic sorting on the chemical composition of the sediments would be minimal. This is also reflected by the distribution of Fe and Al in the mud/sandy-silt fraction of sediments collected in the estuarine station (S7) across the entire quartz-clay spectrum in the $Al_2O_3/SiO_2$ vs $Fe_2O_3/SiO_2$ ratio plot (Figure 7), reflecting the minimal effect of sorting [6,47]. This is because the relative enrichment of Fe and Al in coarse sand (e.g., S1, S4, and S8) as well as the sandy silt (S7) means that there is no control of grain size on their enrichment. This implies that the enrichment of Fe and Al in Umba River sediments is dominantly attributable to the weathering inputs from the catchment. The enrichment of Fe (>0.20) and Al (>0.40) in estuarine (S7) samples could be attributed to the increased input of these elements from the weathering of quartzo-feldspathic and hornblende-pyroxene rich downstream Karoo Supergroup and younger lithologies ( Figure 1b). These lithologies and their associated minerals are rich in Fe and Al elements in their chemical structure [6,18]. Additionally, the contribution of Karoo
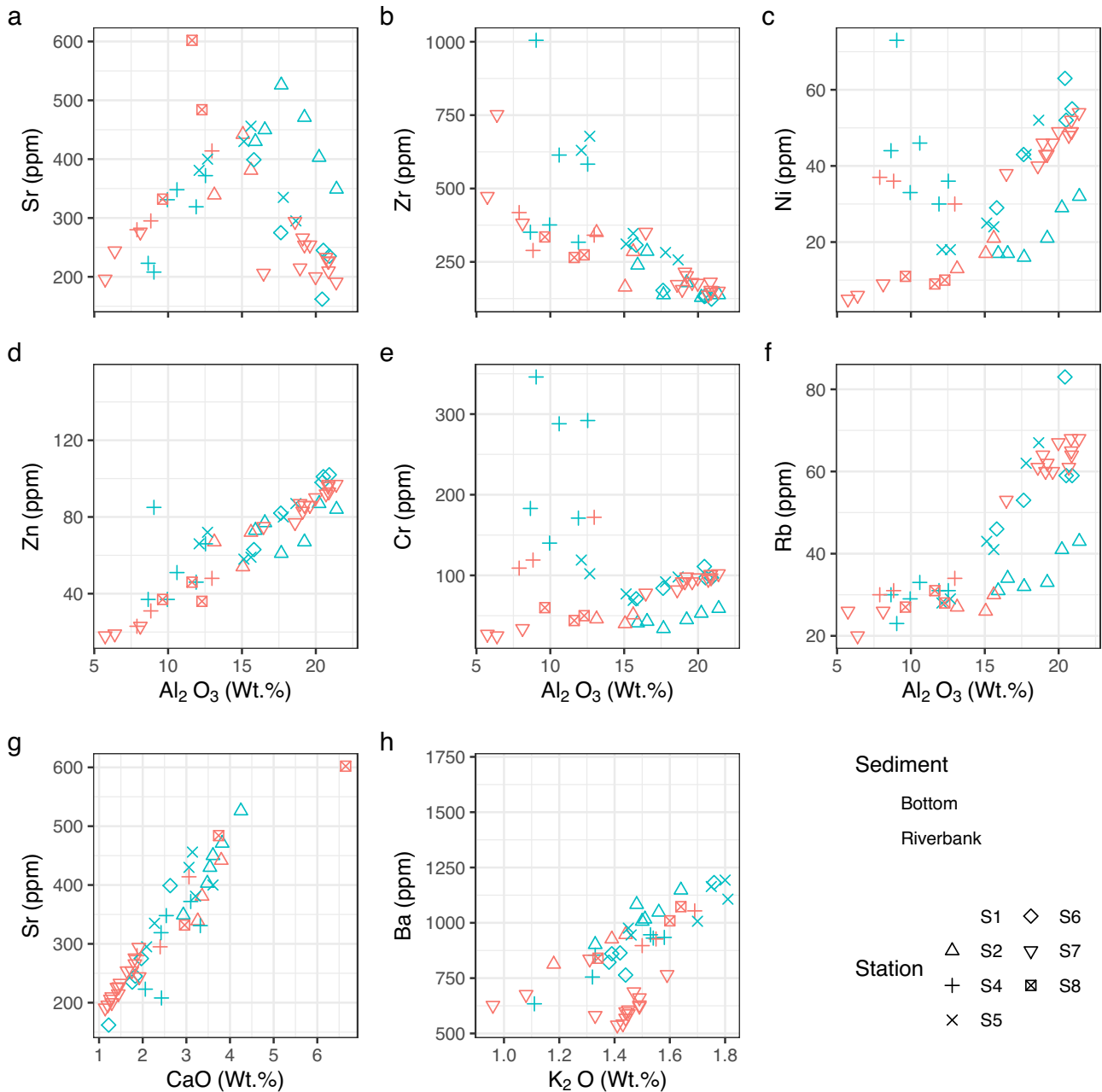
**Figure 8:** Shows the selected trace element variations with respect to the immobile Al$_2$O$_3$ wt% in Umba River sediments. Sr shows positive but scattered (a) relation compared with Zr which shows negative relation with Al$_2$O$_3$ (b). Ni, Zn, Cr, Rb, and Rb (in ppm) show good positive relation with Al$_2$O$_3$ in both the riverbank and bottom sediments (c–f, respectively). Sr (g) and Ba (h) maintain a positive relation with alkali CaO and MgO, respectively, with relatively low Sr and Ba (in ppm) in the bottom estuarine sediments.

Supergroup lithologies to the increased input of Fe and Al would be further promoted by a hot and humid climate due to the proximity to the Indian Ocean relative to upper catchment stations [6]. The similarity of SiO$_2$ – the lack of either enrichment or depletion – relative to UCC further indicates the reduced influence of hydrodynamic sorting on mineralogical and chemical compositions of Umba River sediments [26,44,54].

## 5.2 Weathering indices and source area characteristics

The strong but negative relation between SiO$_2$ and Al$_2$O$_3$ (Figure 6a), the positive relation between Fe$_2$O$_3$ and Al$_2$O$_3$ (Figure 6c), and the positive relation between both Al$_2$O$_3$ and Fe$_2$O$_3$ with CIA (Figure 10a and b), indicate a shift that is expected from the replacement of easily
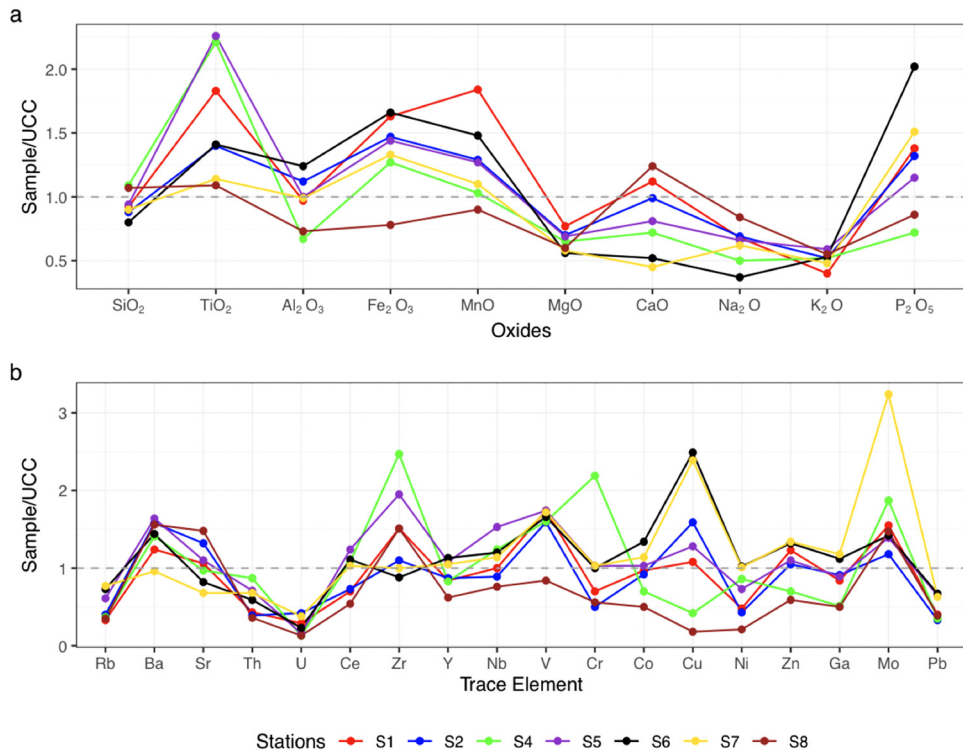
**Figure 9:** Major element oxides (a) and trace element (b) spider plot of Umba sediments normalized against the UCC values from Rudnick and Gao [43]. Major elements are normalized as oxides and trace elements as ppm. Mobile major elements (MgO, CaO, $Na_2O$, and $K_2O$) and trace elements (Rb, Th, and U) are depleted relative to UCC.

weathered minerals towards a dominance of less mobile minerals, e.g., kaolinite composed of mainly the immobile $Al^{3+}$. The positive relation between $Al_2O_3$ and high CIA (Figure 10a) values in both the riverbank and bottom sediments could be attributed to the initial weathering of sediments before the grains enter the fluvial system. Generally, fluvial sediments exhibit CIA values of ~50 at the onset of weathering of a predominantly metamorphic and igneous source geology similar to the Umba River catchment. This value increases with reworking processes during transportation [40,41]. The UCC has a mean CIA of ~47 [44]; however CIA values >70 have also been reported to characterize intense weathering of source rock [49]. According to Campodonico et al. [39], reworked fluvial sediments – through weathering, transport, deposition, and diagenesis – have average CIA values of ~80. Clay minerals, which are an indicator of extensive weathering and chemical alteration, have CIA values close to 100 [37,39]. The large variation in CIA of the Umba River sediments ranging between 39 and 81, with a majority >50 (Figure 11), signifies a low to high degree of weathering. This can be attributed to varying physico-chemical parameters including temperature, salinity, and pH that vary along the longitudinal cross-section of the Umba River [6,51]. The large variation

in CIA values can also be attributed to the supply of pristine material to the fluvial system, supported by the smaller catchment of the Umba River and the short transport from source to mouth. However, the few high alterations recorded can be attributed to the alteration and input of feldspathic and clay minerals dominant in the downstream geology comprised of the Karoo Supergroup. The varying climate from the cold mountainous upstream to the hot and semi-arid midstream, and the hot and humid climate near coastal downstream could explain the variation in CIA [6]. Low CIA values have been reported to be related to low weathering at source due to cooler conditions [34] characteristic of higher elevations, e.g., mountainous regions and semi-arid conditions [6]. These conditions are similar to the Umba River catchment near the source of the river in the Usambara and Pare mountains (Figures 1b and 2). The likely presence of clay minerals, e.g., illite and kaolinite in the Umba River sediments as discussed in Section 4.2 and as observed in the grain size distribution (Table 1), could further explain the CIA variation. Additionally, the observed decrease in lithoclasts and the increase in grains made up of individual mineral crystals from source to mouth (Figures 4 and 5) can indicate the gradual weathering with time exacerbated by river transport. The
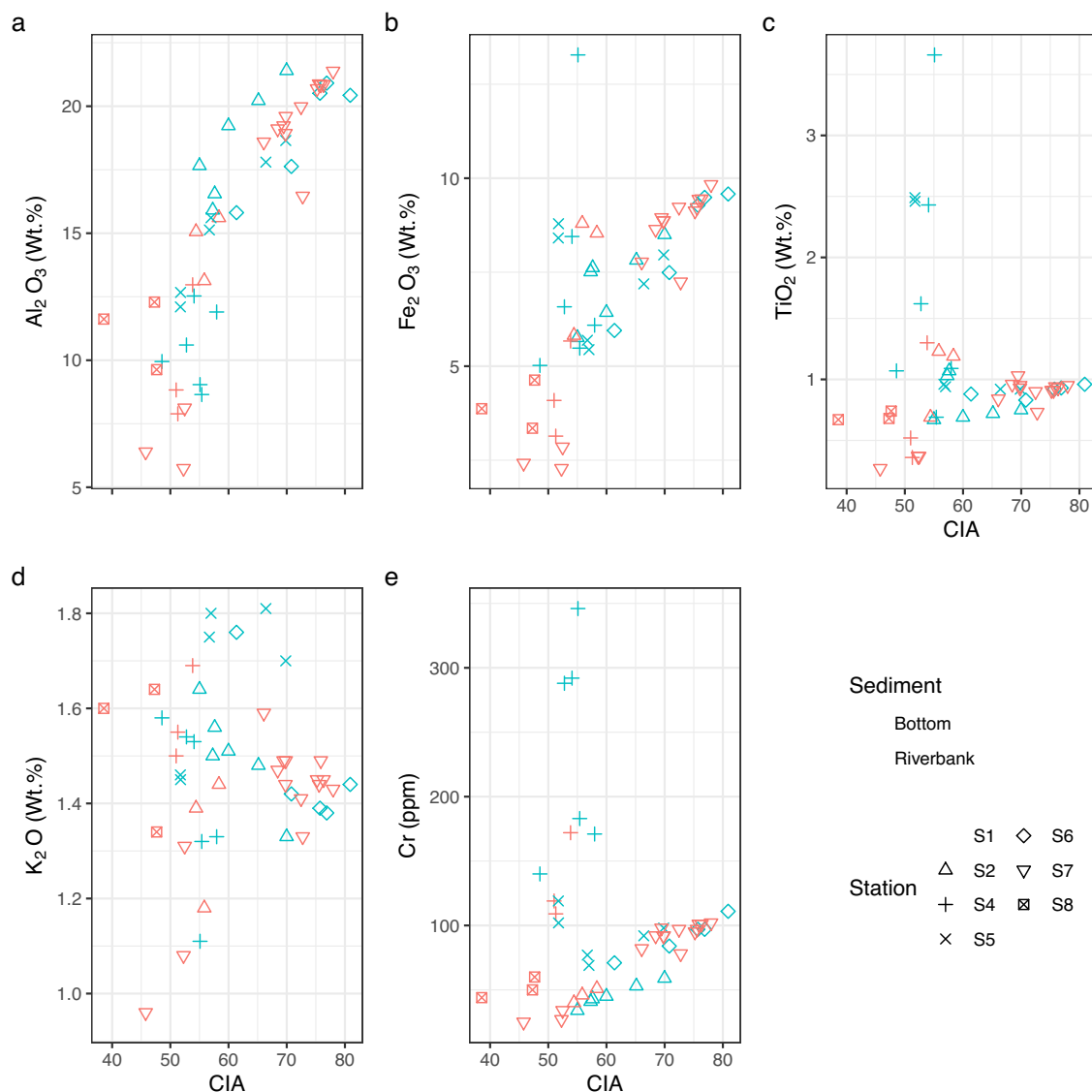
**Figure 10:** Plots of selected major elements namely (a) Al₂O₃ , (b) Fe₂O₃, (c) TiO₂, (d) K₂O and trace element, (e) Cr versus the chemical weathering index (CIA) of Umba River sediments. CIA are defined as (Al₂O₃/[Al₂O₃ + CaO + Na₂O + K₂O]) x 100 in molecular proportions [41,45]. Bottom estuarine samples (S7) show high major oxides variation at different values of CIA. Immobile and less soluble elements (Al₂O₃, TiO₂, and Cr) increases with the increase in CIA (a, c, and e, respectively).

different roundness of grains within the downstream sediments (Figure 5) indicate that some clasts are incorporated in the bulk sediment later than others during fluvial transport. Part of these sediments, thus, have been minimally influenced by river transport; however, in the marine river mouth, wave action is expected resulting in increasing roundness of the grains.

The relatively low weathering in the downstream sediments compared to the upstream sediments, could be attributed to *in situ* and proximal deposition devoid of fluvial transportation. Additionally, the occurrence of poorly rounded quartz mineral grains, being physically

and chemically resistant to weathering (Figures 4 and 5), is consistent with moderate reworking by river transport (Table 1 and Figure 3). The persisting presence of detrital feldspars (plagioclase and K-feldspars), a precursor of clay minerals, is an indication of low weathering of the gneissic granite, igneous, and meta-igneous rocks sourced from the catchment.

The Umba River sediments are plotted across the plagioclase- K-feldspar line and reveal a narrow near-linear trend along the A-CN edge (Figure 11a). This trend has been attributed to possible higher removal rates of Na⁺ and Ca²⁺ from plagioclase compared to K⁺ removal rates
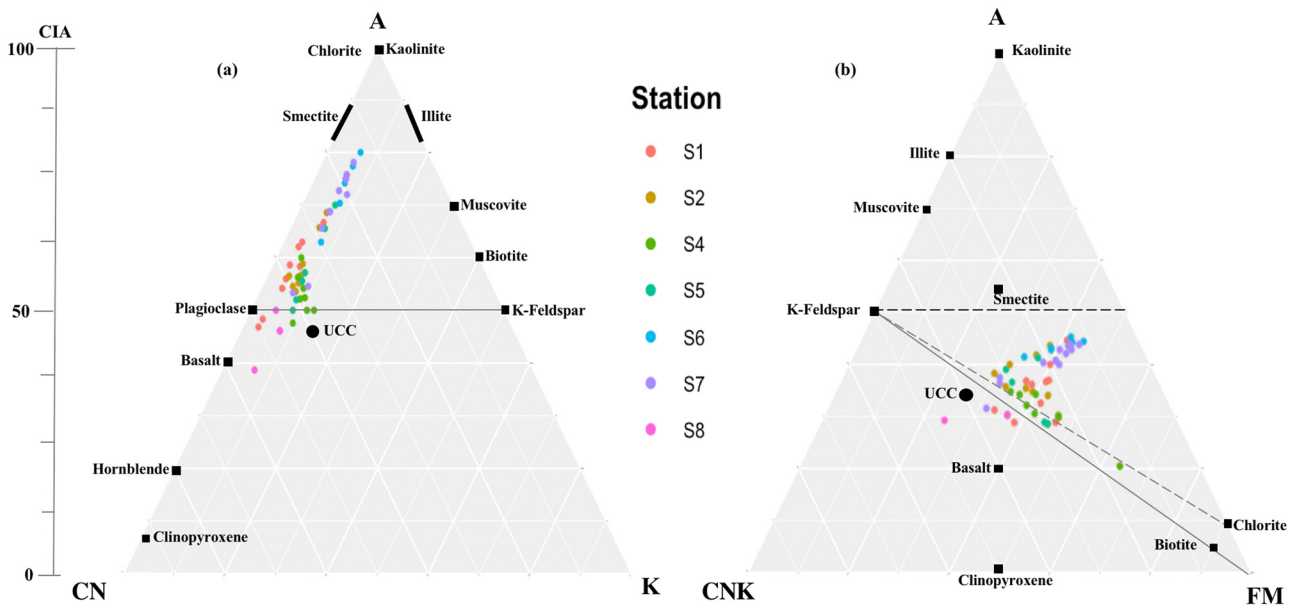
**Figure 11:** Ternary diagrams showing the common primary and secondary minerals and weathering trends of Umba River sediments. The CIA of Umba River sediments range from 39–81 with majority >50. (a) On A-CN-K, Umba River sediments plot along a linear trend on the A-CN edge. (b) On A-CNK-FM, the sediments plot below the smectite field. A = $Al_2O_3$, CN = CaO* + $Na_2O$, K = $K_2O$, CNK = CaO* + $Na_2O$ + $K_2O$, and FM = $Fe_2O_3$ + MgO. Average values of basalt, UCC, and clinopyroxene taken from ref. [3].
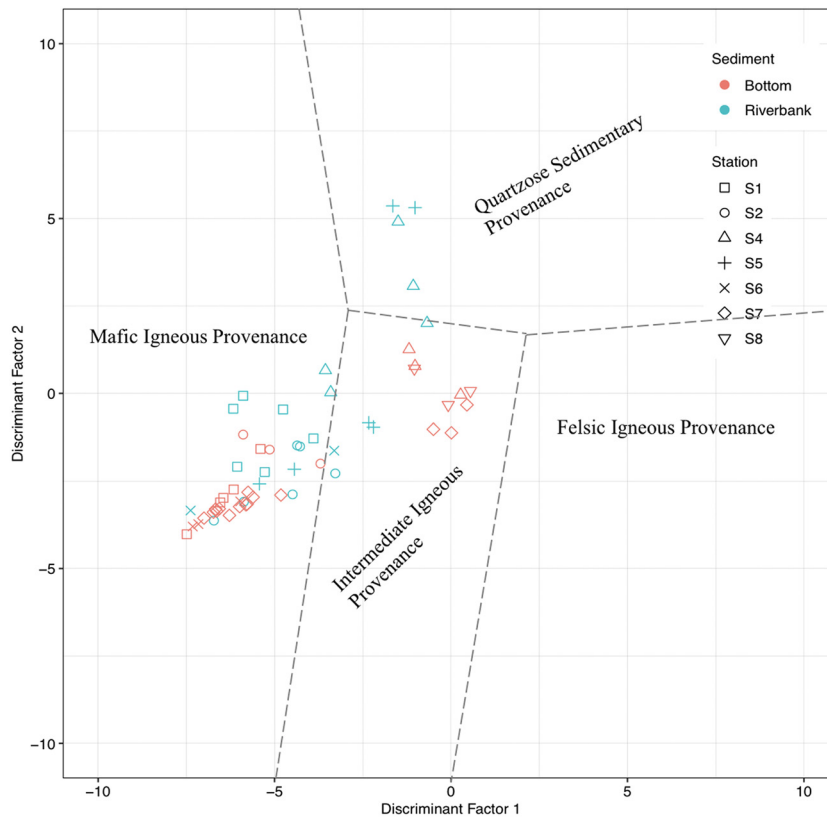


**Figure 12:** Major element provenance DF plot. Major elements-based oxide ratios for the provenance signatures of Umba River sediments [35] plotted across three provenance fields with majority in the mafic and intermediate igneous provenance.

during weathering, transport, and other diagenetic processes [34,49]. However, the linear trend parallel to the A-CN axis could be attributed to the supply and input of relatively pristine sediments to the fluvial system [50]. This is consistent with the relatively short course of the Umba River and the small catchment it drains, consequently allowing faster delivery of newly weathered and pristine material into the fluvial sediments. On the A-CNK-FM, the sediments are plotted below the smectite and K-feldspar field and away from the CNK-FM edge (Figure 11b) further indicating a strong variable degree of weathering of the Umba River sediments. This corroborates the other findings that indicate high variability in weathering and reworking, attributed to progressive sediment input into the river and to varying climatic conditions along its course.

## 5.3 Source characteristics from bulk geochemical composition

In order to make inter-oxide comparisons, the abundance of $Al_2O_3$ was used as a reference factor, mainly because it is immobile and less soluble [34]. High positive inter-oxide relations are observed in the element bivariate plots between the immobile oxide $Al_2O_3$ and $SiO_2$, $Fe_2O_3$, and $P_2O_5$ (Figure 6a, c, and d) in both the riverbank and bottom sediments. This can be attributed to less preferential fractionation during various sedimentary processes including weathering, transportation, and deposition [7,52,53]. It can also be the result of a relatively uniform source geology [26] that would have similar mineralogy as reflected by these elements and observed in the mineral distribution (Figures 4 and 5). This preposition is further supported by the aforementioned influence of the relatively short course of the Umba River that drains a small catchment, limiting the amount of rock lithologies it crosses and therefore, providing a uniform mineralogical and elemental composition. Short rivers tend to transport fresh sediments from source to mouth in a relatively short time, consequently reducing the degree of alteration of the chemical composition. The positive relation between $Al_2O_3$ and $Fe_2O_3$, on one hand, and $P_2O_5$ on the other, can be further attributed to abundances of these elements in platy and sheet phyllosilicates. The observed presence of muscovite, biotite, apatite, and clay minerals in the Umba River sediments (Figures 4 and 5) supports this observed trends [18,47].

The bulk chemical composition of the sediments shows a comparable trend with average UCC chemical compositions (Figure 8a) and is similar to earlier studies within the region [18]. The relative depletion of $Na_2O$ and $K_2O$ observed here (Figure 8a) can be attributed to the result of increased leaching of the highly mobile elements and enrichment of the immobile and less soluble elements. Additionally, alkali elements including Na, Mg, Ca, and K are largely lost as clay minerals are formed during weathering [47]. Alteration of Al- and Mg-bearing minerals including plagioclase and phyllosilicates due to water percolation into rock fractures and crevices could accelerate the removal of mobile elements including Ca, Na, K, and Mg [6]. This is also consistent with moderate to high CIA as proxy for chemical weathering, with higher elemental values of these elements. Additionally, the elevated MgO and CaO contents (Figure 6e and g, respectively) coupled with a scattered relation between $K_2O$ and $Al_2O_3$ (Figure 6f), also reflect a mixed source composition and varying degrees of weathering [26]. However, the observed high $K_2O + Na_2O$ (>2.5%) and the relatively low $K_2O/Na_2O$ ratio (<1) in the Umba River sediments (Table 1) indicate an almost equal contribution of K-rich feldspar and Na-rich plagioclase [34,35,42].

Trace element concentrations vary along the longitudinal course of the Umba River in both the riverbank and bottom sediments (Table 1 and Supplementary Information 2). The less distinct and negative relation of Sr and Zr with $Al_2O_3$ (Figure 8a and b) can be attributed to the mixed geology from source to mouth of the Umba River. The weathering of the crystalline rocks of downstream geology (Figure 1) – rich in quartzo-feldspathic rock composition – would introduce increased amounts of Sr-rich K-feldspars and/or biotite to the sediments [55]. Positive covariation and enrichment of Ni, Zn, and Cr with $Al_2O_3$ in Umba River sediments (Figure 8c, d, and e) can be attributed to the dominance of ferromagnesian elements. These elements are rich in mafic minerals dominant in the mafic granulites [6,18,23] observed in the upper reaches of the Umba River in the Usambara Mountains (Figure 1). Cr/Ni has been used to indicate the mafic and ultramafic provenance [6]. Low Cr/Ni values between 1.3 and 1.5 represent an ultramafic provenance. Both the riverbank and the bottom Umba River sediments exhibit Cr/Ni > 2, indicating a dominantly mafic to felsic provenance. The moderate to high abundances of both Ni (Figure 8c) and Cr (see Figure 8e) in both the riverbank and bottom sediments, suggest a mixed source of Umba River sediments. This mixture is occasioned by the changing lithologies and the subsequent variation in mafic and felsic minerals from source to mouth. The relative depletion and significant variation in Sr (Figure 8g) at low CaO and the depletion of Ba (Figure 8h) at moderate CaO in the estuarine bottom sediments have been

attributed to the physicochemical variations (salinity, dissolved oxygen, and temperature) and the grain size [46,56–58]. This is also supported by the significant variation ($p < 0.05$) in the two elements with environmental setting (Supplementary Information 1). However, the observed depletion of Rb, Th, and U in the Umba River sediments (Figure 9b) signifies a magmatic source geology with geochemical affinities of a meta-igneous granulite [18,19,24]. The sandstone lithology dominant in the lower reaches of Umba River (Figure 1b) is known to be low in Rb and Sr [34], therefore explaining the depletion of Rb relative to UCC.

## 5.4 Provenance

The sediments are plotted across three provenance fields, i.e., mafic igneous, intermediate igneous, and quartzose sedimentary provenance fields (Figure 12) with the majority located in the mafic to intermediate igneous field. This indicates a strong influence of the upper and middle catchment geology, and a subordinate contribution of the lower catchment geology that is primarily composed of quartz-rich lithologies (Figure 1b). The Umba River catchment has pockets of mafic to ultra-mafic granulites (in the mountainous Mng'aro region) and mafic hornblende-pyroxene facies within the Karoo [18,24] further downstream (Figure 1b). On the contrary, the lower catchment is dominated by quartzo-feldspathic-rich sandstones and siltstones that would explain the placement of some Umba River sediments in the quartzose provenance field (Figure 12). Further, the plot in the quartzose sedimentary provenance quadrant suggests the derivation of the Umba River sediments from a recycled orogen [34,35] – presumably, because the upstream Umba River is characterized by the geologically uplifted Usambara mountains [18,20,21].

## 6 Conclusion

The provenance of the sediments deposited along the course of the Umba River from source to mouth have been characterized using a combination of geochemical proxies and petrography. The chemical composition and elemental abundance of riverbank versus bottom sediments of Umba River are significantly different; however, they show similar abundance and distribution trends along the course. The effect of hydrodynamic sorting on the chemical and mineralogical compositions of Umba River sediments is minimal, with the distribution of elements majorly attributed to inputs from weathering. The source geology, relative length of the river, and the small catchment have a dominant influence on the element and mineral compositions and abundances. These assessments has revealed that the Umba River sediments have a predominantly gneissic granite petrology consistent with the underlying catchment geology, characterized by a Precambrian craton and the Karoo Supergroup in its upper reaches and the much younger Cenozoic outcrops and Quaternary sediments further downstream towards the coast. The Umba River sediments also exhibit a UCC-like chemical composition and further geochemical preservation of source characteristics, reflected by the similarity of mineralogy of upstream riverine sediments (close to source) and downstream sediments (estuarine). This is further supported by the moderate to high alteration reflected by the CIA, evident by the marked depletion of mobile and labile elements like MgO, CaO, Na$_2$O, K$_2$O, and Sr relative to UCC.

**Author contributions:** Study conception and design: A.K., J.O., J.K., N.K. Acquisition of data: A.K., J.O., O.O. Analysis, interpretation of data, and drafting of manuscript: A.K. Critical revision: H.W., J.O., N.K., J.K.

**Conflict of interest:** The authors declare that the research was conducted in the absence of any commercial or financial relationships that could be construed as a potential conflict of interest regarding the publication of this original manuscript.

**Data availability statement:** The datasets generated during and/or analysed during and for the current study are available from the corresponding author on reasonable request.

# References

[1] Milliman JD, Bonaldo D, Carniel S. Flux and fate of river-discharged sediments to the adriatic sea. Adv Oceanogr Limnol. 2016;7:106–14.

[2] Lim D, Jung HS, Choi JY. REE partitioning in riverine sediments around the Yellow Sea and its importance in shelf sediment provenance. Mar Geol. 2014;357:12–24.

[3] Wang ZL, Liu CQ. Geochemistry of rare earth elements in the dissolved, acid-soluble and residual phases in surface waters of the Changjiang Estuary. J Oceanogr. 2008;64:407–16.

[4] Cox R, Lowe DR, Cullers RL. The influence of sediment recycling and basement composition on evolution of mudrock chemistry in the southwestern United States. Geochim Cosmochim Acta. 1995;59:2919–40.

[5] Taylor SR, McLennan SM. The continental crust: its composition and evolution. Blackwells: Oxford; 1985. p. 301.

[6] Sensarma S, Rajamani V, Tripathi JK. Petrography and geochemical characteristics of the sediments of the small River Hemavati, Southern India: implications for provenance and weathering processes. Sediment Geol. 2008;205:111–25.

[7] Sarkar SK, Frančišković-Bilinski S, Bhattacharya A, Saha M, Bilinski H. Levels of elements in the surficial estuarine sediments of the Hugli River, northeast India and their environmental implications. Environ Int. 2004;30:1089–98.

[8] Amorosi A. Chromium and nickel as indicators of source-to-sink sediment transfer in a Holocene alluvial and coastal system (Po Plain, Italy). Sediment Geol. 2012;280:260–9.

[9] Ali S, Stattegger K, Garbe-Schönberg D, Frank M, Kraft S, Kuhnt W. The provenance of Cretaceous to Quaternary sediments in the Tarfaya basin, SW Morocco: evidence from trace element geochemistry and radiogenic Nd-Sr isotopes. J Afr Earth Sci. 2014;90:64–76.

[10] Dickinson WR, Beard LS, Brakenridge GR, Erjavec JL, Ferguson RC, Inman KF, et al. Provenance of North American Phanerozoic sandstones in relation to tectonic setting. Geol Soc Am Bull. 1983;94:222–35.

[11] Leleyter L, Probst J-L, Depetris P, Haida S, Mortatti J, Rouault R, et al. Comptes Rendus de l'Académie des Sci-Series IIA-Earth Planet Sci. 1999;329:45–52.

[12] Jung H-S, Lim D, Choi J-Y, Yoo H-S, Rho K-C, Lee H-B. Rare earth element compositions of core sediments from the shelf of the South Sea, Korea: their controls and origins. Continent Shelf Res. 2012;48:75–86.

[13] Mil-Homens M, Vale C, Raimundo J, Pereira P, Brito P, Caetano M. Major factors influencing the elemental composition of surface estuarine sediments: the case of 15 estuaries in Portugal. Mar Pollut Bull. 2014;84:135–46.

[14] Funk C, Hoell A, Shukla S, Husak G, Michaelsen J. The East African monsoon system: seasonal climatologies and recent variations. The monsoons and climate change. Cham: Springer; 2016. p. 163–85.

[15] Fortnam M, Atkins M, Brown K, Chaigneau T, Frouws A, Gwaro K, et al. Multiple impact pathways of the 2015–2016 El Niño in coastal Kenya. Ambio. 2021;50(1):1–16.

[16] Daron JD, Sutherland K, Jack C, Hewitson BC. The role of regional climate projections in managing complex socio-ecological systems. Regional Environ Change. 2015;15:1–12.

[17] The International Union for Conservation Network (IUCN). Eastern Africa programme 2003: The Pangani Basin: a situation analysis; 2003. p. 104, xvi.

[18] Maboko MAH, Nakamura E. Isotopic dating of Neoproterozoic crustal growth in the Usambara mountains of northeastern Tanzania: evidence for coeval crust formation in the Mozambique belt and the Arabian-Nubian Shield. Precambrian Res. 2002;113:227–42.

[19] Schlüter T. Geology of East Africa. XII. Stuttgart, Germany: Schweizerbart'sche Verlagsbuchhandlung; 1997.

[20] Mutakyahwa MKD, Ikingura JR, Mruma AH. Geology and geochemistry of bauxite deposits in Lushoto district, Usambara Mountains, Tanzania. J Afr Earth Sci. 2003;36:357–69.

[21] Shackleton R. Tectonics of the lower crust: a view from the Usambara Mountains, NE Tanzania. J Struct Geol. 1993;15:663–71.

[22] Schlünz BSRR. Transport of terrestrial organic carbon to the oceans by rivers: re-estimating flux and burial rates. Int Earth Sci. 2000;88:599–606.

[23] Manya S, Maboko MAH, Nakamura E. Geochemistry and Nd-isotopic composition of potassic magmatism in the Neoarchaean Musoma-Mara Greenstone Belt, northern Tanzania. Precambrian Res. 2007;159:231–40.

[24] Akech NO, Omuombo CA, Masibo M. General geology of Kenya. In: Paron P, Olago DO, Omuto CT, editors. Kenya a national outlook geo-environmental resource hazards, 16th ed. Developments in earth surface processes. Amsterdam, Netherlands: Elsevier B.V; 2013. p. 3–10.

[25] Cairncross B, Mössmer T, editors. Minerals and gemstones of East Africa. Cape Town: Pippa Parker; 2019.

[26] Hossain HMZ, Kawahata H, Roser BP, Sampei Y, Manaka T, Otani S. Chemie der Erde Geochemical characteristics of modern river sediments in Myanmar and Thailand: Implications for provenance and weathering. Chem der Erde. 2017;77:443–58.

[27] Folk RL, William Ward XC. Brazos river bar [Texas]: a study in the significance of grain size parameters. J Sediment Res. 1957;27(1):3–26.

[28] Camuti KS, McGuire PT. Preparation of polished thin sections from poorly consolidated regolith and sediment materials. Sediment Geol. 1999;128:171–8.

[29] Murphy CP. Thin section preparation of soils and sediments. United Kingdom: AB Academic Publishers; 1986.

[30] Gupta JGS, Bertrand NB. Direct ICP-MS determination of trace and ultratrace elements in geological materials after decomposition in a microwave oven. Part II. Quantitation of Ba, Cs, Ga, Hf, In, Mo, Nb, Pb, Rb, Sn, Sr, Ta and Ti. Talanta. 1995;42(12):1947–57.

[31] Pruseth KL, Yadav S, Mehta P, Pandey D, Tripathi JK. Problems in microwave digestion of high-Si and high-Al rocks. Curr Sci. 2005;89:1668–71.

[32] Zhuchenko NA, Chebykin EP, Stepanova OG, Chebykin AP, Gol'Dberg EL. Microwave digestion of bottom sediments from lake Baikal for the inductively coupled plasma mass-

spectrometric determination of their elemental composition. J Anal Chem. 2008;63:943–9.

[33] Zindorf M, März C, Schnetger B. Data report: wavelength-dispersive X-ray fluorescence–based geochemical data, Site U1418, IODP Expedition 341, Gulf of Alaska. Jaeger JM, Gulick SPS, LeVay LJ. Exped 341 Sci Proc Integr Ocean Drill Program, 341 Coll Station TX (Integrated Ocean Drill Program); 2020.

[34] Baiyegunhi C, Liu K, Gwavava O. Geochemistry of sandstones and shales from the Ecca Group, Karoo supergroup, in the eastern cape province of South Africa: implications for provenance, weathering and tectonic setting . Open Geosci. 2017;9:340–60.

[35] Bhat NA, Singh BP, Bhat AA, Nath S, Guha DB. Application of geochemical mapping in unraveling paleoweathering and provenance of Karewa deposits of South Kashmir, NW Himalaya, India. J Geol Soc India. 2019;93:68–74.

[36] Depetris PJ, Pasquini AI, Lecomte KL. Weathering and the riverine denudation of continents. Dordrecht: Springer Netherlands; 2014.

[37] Shao JQ, Yang SY. Does chemical index of alteration (CIA) reflect silicate weathering and monsoonal climate in the Changjiang River basin? Chin Sci Bull. 2012;57:1178–87.

[38] Shao J, Yang S, Li C. Chemical indices (CIA and WIP) as proxies for integrated chemical weathering in China: inferences from analysis of fluvial sediments. Sediment Geol. 2012;265:110–20.

[39] Campodonico VA, García MG, Pasquini AI. The geochemical signature of suspended sediments in the Parana River basin: implications for provenance, weathering and sedimentary recycling. Catena. 2016;143:201–14.

[40] Nesbitt HW, Young GM. Prediction of some weathering trends of plutonic and volcanic rocks based on thermodynamic and kinetic considerations. Geochim Cosmochim Acta. 1984;48:1523–34.

[41] Nesbitt H, Young G. Early Proterozoic climates and plate motions inferred from major elements chemistry of lutites. Nature. 1982;299:715–7.

[42] Goswami B, Bhattacharyya C. Petrogenesis of shoshonitic granitoids, Eastern India: Implications for the late Grenvillian post-collisional magmatism. Geosci Front. 2014;5:821–43.

[43] Rudnick RL, Gao S. Composition of the continental crust. Crust. 2003;3:1–64.

[44] McLennan SM. Weathering and global denudation. J Geol. 1993;101:295–303.

[45] Nesbitt HW, Young GM. Formation and diagenesis of weathering profiles. J Geol. 1989;97:129–47.

[46] He M, Zheng H, Clift PD, Tada R, Wu W, Luo C. Geochemistry of fine-grained sediments in the Yangtze River and the implications for provenance and chemical weathering in East Asia. Prog Earth Planet Sci. 2015;2(1):1–20.

[47] Wu W, Xu S, Lu H, Yang J, Yin H, Liu W. Mineralogy, major and trace element geochemistry of riverbed sediments in the headwaters of the Yangtze, Tongtian River and Jinsha River. J Asian Earth Sci. 2011;40:611–21.

[48] He M, Zheng H, Huang X, Jia J, Li L. Yangtze River sediments from source to sink traced with clay mineralogy. J Asian Earth Sci. 2013;69:60–9.

[49] Mishra M, Sen S. Provenance, tectonic setting and source-area weathering of Mesoproterozoic Kaimur Group, Vindhyan Supergroup, Central India. Geol Acta. 2012;10:283–93.

[50] Borges JB, Huh Y, Moon S, Noh H. Provenance and weathering control on river bed sediments of the eastern Tibetan Plateau and the Russian Far East. Chem Geol. 2008;254:52–72.

[51] Greber ND, Dauphas N. The chemistry of fine-grained terrigenous sediments reveals a chemically evolved Paleoarchean emerged crust. Geochim Cosmochim Acta. 2019;255:247–64.

[52] Fiantis D, Nelson M, Shamshuddin J, Goh TB, Van, Ranst E. Determination of the geochemical weathering indices and trace elements content of new volcanic ash deposits from Mt. Talang (West Sumatra) Indonesia. Eurasian Soil Sci. 2010;43:1477–85.

[53] Silva MM, Pinto MM, Carvalho PC. Major, trace and REE geochemistry of recent sediments from lower Catumbela River (Angola). J Afr Earth Sci. 2016;115:203–17.

[54] Garzanti E, Andò S, France-Lanord C, Vezzoli G, Censi P, Galy V, et al. Mineralogical and chemical variability of fluvial sediments. 1. Bedload sand (Ganga-Brahmaputra, Bangladesh). Earth Planet Sci Lett. 2010;299(3–4):368–81.

[55] Garzanti E, Andò S, Limonta M, Fielding L, Najman Y. Diagenetic control on mineralogical suites in sand, silt, and mud (Cenozoic Nile Delta): implications for provenance reconstructions. Earth-Sci Rev. 2018;185:122–39.

[56] He S, Xu YJ. Concentrations and ratios of dissolved Sr, Ba and Ca along an estuarine river to the Gulf of Mexico-implication for sea level rise effects on trace metal distribution. Biogeosci Discuss. 2015;12:18425–61.

[57] Wang A, Wang Z, Liu J, Xu N, Li H. The Sr/Ba ratio response to salinity in clastic sediments of the Yangtze River Delta. Chem Geol. 2021;559:119923.

[58] He S, Xu YJ. Spatiotemporal distributions of Sr and Ba along an estuarine river with a large salinity gradient to the Gulf of Mexico. Water (Switz). 2016;8:323.